



Preparation of activated carbon based on hair and its selectively removing ability for Fe(III) from La(III)

Hu-Fei Li, Wang Yong, Tuo-Ping Hu, Jian-Feng Gao, Fu-Qiang An*

Chemical Department, North University of China, Taiyuan 030051, China, Tel. 86-351-3923197; Fax: 86-351-3922118; emails: anfuqiang@nuc.edu.cn (F.-Q. An), 850241860@qq.com (H.-F. Li), 864869903@qq.com (Y. Wang), tuopinghu@126.com (T.-P. Hu), gaojianfeng@163.com (J.-F. Gao)

Received 29 May 2019; Accepted 10 November 2019

ABSTRACT

It is of great significance to effectively remove impurity such as Fe from rare earth elements because the trace of Fe(III) have serious damage to the performance of rare earth materials. In this study, a hair-based activated carbon (ACH*) was synthesized and characterized by surface area analyzer, Fourier transform infrared spectroscopy and elemental analysis. The identification and removal of the performance of ACH600 for Fe(III) in the La(III) solution was studied. The adsorption capacity of ACH600 for Fe(III) was 15.54 mg/g and the removal rate reached up to 98.6% by virtue of abundant nitrogen-containing functional group. The selectivity coefficient of ACH600 for Fe(III) was 8.3 relative to La(III). In addition, the ACH600 also has good regeneration and reusability.

Keywords: Activated carbon; Selectively; Adsorption; Fe(III); Hair

1. Introduction

Rare earth elements as a valuable strategic resource, are widely used in metallurgy, military, new materials and other fields [1], in which high-purity of rare earths is indispensable [2–6]. Therefore, it is extremely important to effectively remove non-rare earth impurities in rare earths. To date, solvent extraction, ion exchange, and extraction chromatography are commonly applied in the removal of impurities. However, the practical application of each approach was limited by its disadvantages [7–10]. Solvent extraction may cause wide-spreading and persisting pollution due to the extensive use of the organic phase. The ion exchange process is time-consuming and unsuitable for industrial production. Extraction chromatography consumes a large amount of acid and requires a purification device in mass production, which results in low economic efficiency. Comparing with the above mentioned traditional method, the adsorption method is

more popular due to its higher efficiency, better repeatability and lower costs [11–15].

Activated carbon has been deemed as one of the most promising adsorbents, owing to its large specific surface area and flexible surface functional groups [16–25]. Based on these characteristics, the activated carbon synthesized by the special method has been applied to the separation of substances in wastewater. AC-P700 was obtained by the activation of pea and was used in the elimination of aluminum from the lanthanum solution. The experimental results showed that the adsorption capacity of aluminum reached 0.53 mmol g⁻¹ demonstrating the excellent capability of activated carbon for the removal of trace amounts of aluminum [26].

In this study, nitrogen-doped activated carbon was manufactured using hair and was characterized by surface area analyzer, elemental analysis, and Fourier transform infrared spectroscopy (FTIR). The adsorption tests of as-prepared activated carbon for Fe(III) and La(III) were performed.

* Corresponding author.

The influences of pH values, contact time, adsorbent dose, and the ion concentration on adsorption ability were investigated.

2. Experimental

2.1. Material

Hair was collected from a barbershop in the North University of China. NaOH, FeCl₃. All reagents were analytical (AR) grade.

2.2. Preparation and characterizations of ACH400, ACH500, ACH600

Firstly, hair was washed by distilled water and dried at 353 K for 24 h. Then, 5 g of hair was soaked in 500 ml of NaOH aqueous solution with a concentration of 10 g L⁻¹ for 24 h. After filtrated and dried, the resultant hair was carbonized in a charcoal furnace at 873 K for 2 h with a heating rate of 2 K min⁻¹ and N₂ flow of 50 mL min⁻¹. Finally, the resultant samples were washed with distilled water until the filtrate was neutral and dried at 353 K for 24 h in a vacuum oven. The obtained material is expressed in ACH* (*represents carbonization temperature, such as ACH400, ACH600).

N₂ adsorption–desorption curves of ACH600 were measured using surface area analyzer (Beijing JWGB BF-JW132F) by nitrogen adsorption at 77 K. Before measured, the sample was degassed under vacuum at 593 K for 2 h. FTIR spectra were performed on Nicolet FTIR 4800s (Shimadzu, Japan) spectrometer using the traditional KBr pellet technique. The element content was measured using Vario EL elemental analyzer (Elementar, Germany).

2.3. Batch adsorption experiments of activated carbon towards Fe(III)

2.3.1. Adsorption experiments

0.01 g of ACH400, ACH500, ACH600 was directly introduced into a conical flask containing 20 mL Fe(III) aqueous solution with initial concentration (C₀) of 40 mg L⁻¹ and pH of 2.5. Then the conical flask was placed in a thermostatic water bath oscillator. The adsorbent was separated from the solution by filtration and the concentrations (C_t) of Fe(III) solution was measured with inductively coupled plasma emission spectrometer.

The adsorption capacity (Q, mg g⁻¹) was calculated according to Eq. (1). In this study, the effects of adsorption time, initial concentration, pH, and the dosage of adsorbent on adsorption capacity and ion removal efficiency (R) were investigated, respectively.

$$Q = \frac{V(C_0 - C_t)}{m} \quad (1)$$

$$R = \frac{(C_0 - C_t)}{C_0} \times 100\% \quad (2)$$

where C₀ is the initial concentration (mg L⁻¹); C_t is the concentration at the t moment (mg L⁻¹); V is the volume of solution (L); m is the dosage of adsorbent ACH* (g); R is the removal rate.

2.3.2. Competitive adsorption experiment

The competitive adsorptions were carried out by a batch method. ACH* was added into a binary mixed solution of Fe(III) and La(III). After adsorption reached equilibrium, the concentrations of all metal ions in the remaining solutions were determined. Distribution coefficients (K_d) of Fe(III) and La(III) were calculated by Eq. (3). Selectivity coefficient (k) of ACH600 towards Fe(III) with respect to the species of competitor La(III) was calculated according to Eq. (4).

$$K_d = \frac{Q_e}{C_e} \quad (3)$$

$$k = \frac{K_d(\text{Fe})}{K_d(\text{La})} \quad (4)$$

2.3.3. Adsorption dynamics experiment

ACH600 was firstly filled in a glass column with a volume of 10 mL. Then the mixture solution of Fe(III) and La(III) was allowed to flow gradually through the column at a rate of 5 BV h⁻¹. The initial concentrations of Fe(III) and La(III) were 10 and 100 mg L⁻¹, respectively, and pH was adjusted as 2.5. The effluent was collected and concentration was determined. Then the adsorption dynamics curve was plotted.

2.3.4. Reusability tests

Reuse performance is an important factor in its application. The ACH600 that saturatedly adsorbed Fe(III) was washed using 3 mol L⁻¹ of nitric acid solution for 2 h. The Fe(III) adsorbed on ACH600 is eluted, and the carbon material regenerates. Then adsorption-desorption experiments were repeated to test the reusability of ACH600.

3. Results and discussion

3.1. Characterization

The N₂ adsorption-desorption isotherms and pore size distribution curves are shown in Fig. 1. The pore properties of ACH600 are listed in Table 1. It could be seen from Fig. 1 that the adsorption curve of ACH600 exhibited a typical type II isotherm with a small hysteresis loop of type H₃, and the N₂ adsorption curve is coincident with the desorption curve. The results show that ACH600 has a large mesoporous structure and a wide range of pore size distribution, which was in agreement with the aperture distribution curve. There were many peaks in the pore size distribution curve, indicating that the pore distribution of ACH600 is not uniform. As can be seen from Table 1, ACH600 has a relatively developed pore structure and rich nitrogen-containing functional groups. Heavy metal ions could be adsorbed by activated carbon-containing amino groups [25,32].

3.2. Fourier transform infrared spectroscopy

FTIR spectra of ACH600 is illustrated in Fig. 2. As can be seen from Fig. 2, the peak appeared at 1,540 and 3,430 cm⁻¹

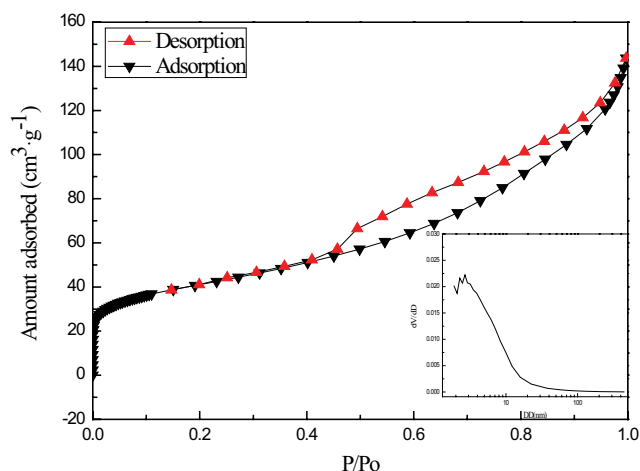


Fig. 1. N_2 adsorption-desorption isotherms and pore size distribution curve.

Table 1
Pore structure parameters

Surface properties			Elemental analysis		
S_{BET}	Pore volume	Pore size	N%	C%	H%
($\text{m}^2 \text{g}^{-1}$)	($\text{cm}^3 \text{g}^{-1}$)	(nm)	–	–	–
145.46	0.22	6.12	1.94	2.72	1.82

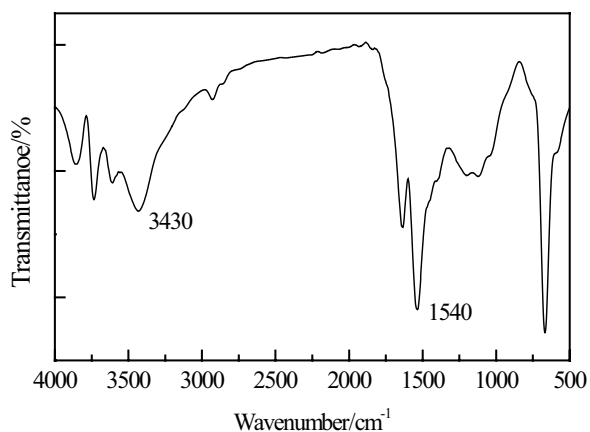


Fig. 2. FTIR spectra.

can be assigned to the deformation vibration and stretching vibration of the N–H bond, respectively. This indicates that some amino groups were retained after activated carbonization.

3.3. Kinetics adsorption curve

The adsorption kinetics of ACH400, ACH500 and ACH600 towards Fe(III) and La(III) are shown in Figs. 3a and b. The adsorption towards Fe(III) and La(III) ions reached equilibrium within 75 and 100 min, respectively. The saturated

adsorption capacity of ACH600 for Fe(III) and La(III) is 15.54 and 6.78 mg g^{-1} , respectively. It was implied that ACH600 possesses very strong adsorption ability towards Fe(III). The reason is that the ACH600 has developed pore structure and abundant surface functional groups, and Fe(III) ion could quickly pass the pore and combine with the active site (mainly amino groups) [33].

To further understand the adsorption kinetics of Fe(III) and La(III) on ACH600, The experimental data were fitted by the Lagergren-first-order, pseudo-second-order and intraparticle diffusion model, and the results are listed in Table 2.

Lagergren-first-order:

$$\ln(Q_{e,1} - Q_t) = \ln Q_{e,1} - k_1 t \quad (5)$$

Pseudo-second-order:

$$\frac{t}{Q_t} = \frac{1}{(k_2 Q_{e,2}^2)} + \frac{t}{Q_{e,2}} \quad (6)$$

Intraparticle diffusion model:

$$Q_t = k_{\text{id}} t^{1/2} + C \quad (7)$$

where Q_e and Q_t (mg g^{-1}) are the equilibrium adsorption capacity and adsorption capacity at time t , respectively; k_1 (min^{-1}), k_2 ($\text{g mg}^{-1} \text{min}^{-1}$), and k_{id} ($\text{mg g}^{-1} \text{min}^{1/2}$) are the rate constant of Lagergren-first-order, pseudo-second-order, and intra-particle diffusion models; C (mg g^{-1}) is a constant related to the thickness of the boundary layer.

From the linear correlation coefficient in Table 3, the adsorption of Fe(III) and La(III) on ACH600 obeys the pseudo-second-order kinetics model well. It can be concluded that the adsorption processes of Fe(III) and La(III) are mainly related to the amount of adsorbent and the concentration of the solution.

3.4. Adsorption isotherm

The adsorption isotherms of ACH600 towards Fe(III) is presented in Fig. 4. To further explore the adsorption mechanism, both Langmuir and Freundlich models are applied to interpret the experimental data, and the result is listed in Table 3.

Langmuir equation:

$$\frac{C_e}{Q_e} = \frac{C_e}{Q} + \frac{1}{KQ} \quad (8)$$

Freundlich equation:

$$\ln Q_e = \ln k + \left(\frac{1}{n}\right) \ln C_e \quad (9)$$

where Q_e (mg g^{-1}) is the equilibrium adsorption capacity, Q (mg g^{-1}) is the theoretical adsorption capacity, C_e (mg L^{-1}) is the equilibrium concentration, K (L g^{-1}) is the Langmuir adsorption constant relating to the free energy of adsorption, k and n are the Freundlich parameters.

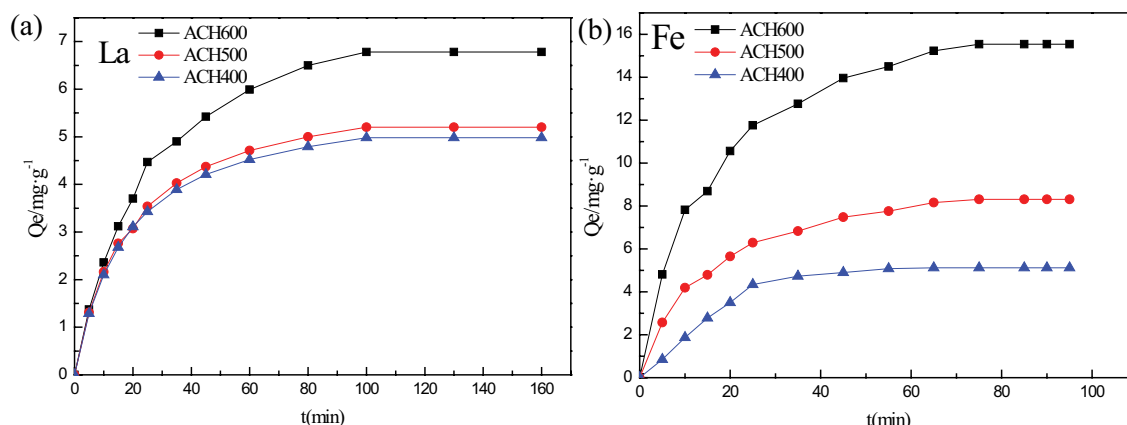


Fig. 3. Adsorption kinetics curves ($T = 25^{\circ}\text{C}$ and $\text{pH} = 2.5$).

Table 2
Comparison of Fe^{3+} adsorption onto ACH600 other adsorbents

Number	Adsorbents	Q_e (mg g^{-1})	Adsorption condition		Reference
			T ($^{\circ}\text{C}$)/ PH /	t (min)	
1	ACUF700	13	25/2/100		[27]
2	FCS/AC	11.07	25/5/400		[28]
3	Tannic acid	1.77	25/4/60		[29]
	Immobilized activated carbon				
4	Activated carbon	0.019	/7/		[30]
5	Ch-P	9.88	25/3.5/120		[31]
6	Porous carbon	0	30/		[25]
7	ACH600	15.54	25/2.5/75		This study

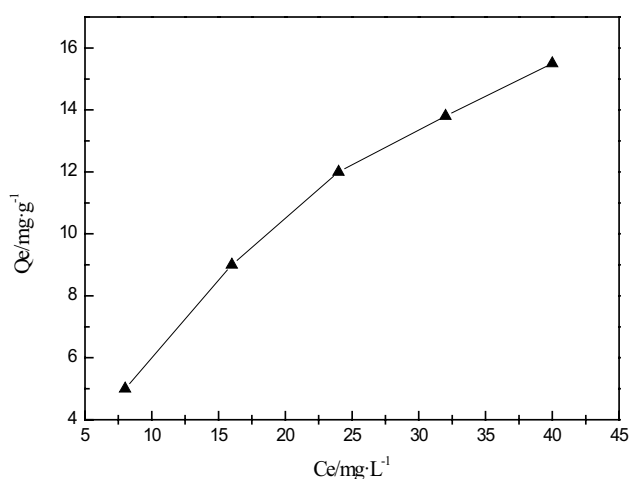


Fig. 4. Adsorption isotherm of ACH600 towards $\text{Fe}(\text{III})$ ($T = 25^{\circ}\text{C}$ and $\text{pH} = 2.5$).

From Table 4 it can be seen that the R^2 for the Langmuir and Freundlich models were larger than 0.99, implying that both the Langmuir and Freundlich models are suitable for the adsorption of $\text{Fe}(\text{III})$ on ACH600. Thus, the applicability

of monolayer coverage of $\text{Fe}(\text{III})$ on the surface of the activated carbon is confirmed.

3.5. Effect of temperature and pH

Both temperature and pH are important parameters during the absorption process. The influence of temperature is investigated at the range of 289–301 K under a pH of 2.5. As depicted in Fig. 5, the adsorption capacity of ACH600 for $\text{Fe}(\text{III})$ and $\text{La}(\text{III})$ increases with an increase of temperature in 289–301 K, suggesting that adsorption of $\text{Fe}(\text{III})$ and $\text{La}(\text{III})$ is an endothermic process and the elevated temperature is favorable for adsorption. Under the same experimental conditions, the difference of adsorption capacity towards $\text{Fe}(\text{III})$ and $\text{La}(\text{III})$ can be observed, and the gap between the $\text{Fe}(\text{III})$ and $\text{La}(\text{III})$ became larger with as elevating temperature. The difference in adsorption capacities between the $\text{Fe}(\text{III})$ and $\text{La}(\text{III})$ was up to 10 g g^{-1} at a temperature of 300 K. It can also be demonstrated that the coordination interaction between the metal ion and the nitrogen-containing functional group is the main driving force for adsorption. That's because lanthanum has a high molecular weight and can't get through the holes in the ACH600. Therefore, with an increase in temperature, the adsorption of iron increased more rapidly than that of lanthanum. The results show that ACH600 has a good ability for removal of $\text{Fe}(\text{III})$ in $\text{Fe}(\text{III})/\text{La}(\text{III})$ mixed solution.

Table 3
Kinetic parameters and correlation coefficients of three kinetic equations

Ion	Experiment		Fe(III)	La(III)
	Value			
Lagergren-first-order	Q_e	(mg g^{-1})	15.54	6.78
	$Q_{e,1}$	(mg g^{-1})	16.7	9.92
	k_1	(min^{-1})	0.184	0.051
	R^2		0.9947	0.9849
Pseudo-second-order	$Q_{e,2}$	(mg g^{-1})	16	8.26
	k_2	($\text{g}/(\text{mg min}^2)$)	0.036	0.005
	R^2		0.9979	0.9988
Intraparticle diffusion	k_{id}	($\text{mg}/(\text{g min}^2)$)	0.914	0.717
	R^2		0.9835	0.9599

Table 4
Fitting parameters and correlation coefficients of Langmuir and Freundlich equation

Langmuir			Freundlich		
R^2	K (L mg^{-1})	Q_0 (mg g^{-1})	R^2	k	n
0.9989	24.7	32.26	0.9925	1.24	1.44

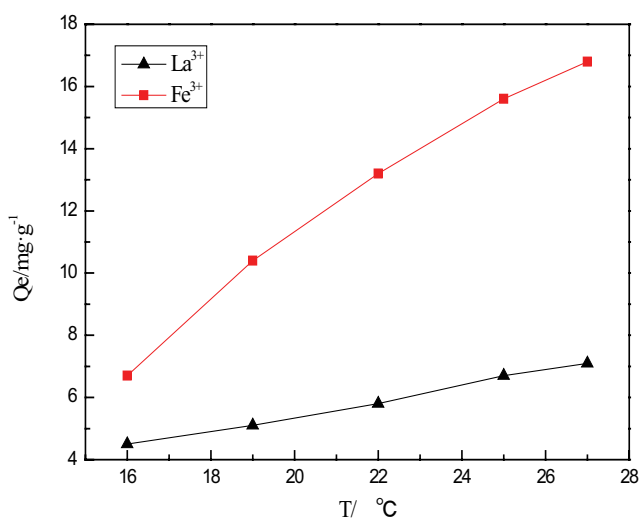


Fig. 5. Effect of temperature on adsorption capacity (pH = 2.5).

The influence of pH on the absorption of the metal ion is studied in the pH values ranging from 1.0 to 3.0. As shown in Fig. 6, the adsorption capacity increases with a rise of pH within the scope of this study. At lower pH values, the N atoms in the material are protonated, leading to lower affinity of the active sites towards heavy metal ions. For another, excessive H^+ also competes with metal ions, resulting in a decrease in adsorption capacity. Hence, with an increase of pH, the protonation degree of N decreases, and the metal ions are more easily combined with the active center on the ACH600, eventually increasing the adsorption capacity.

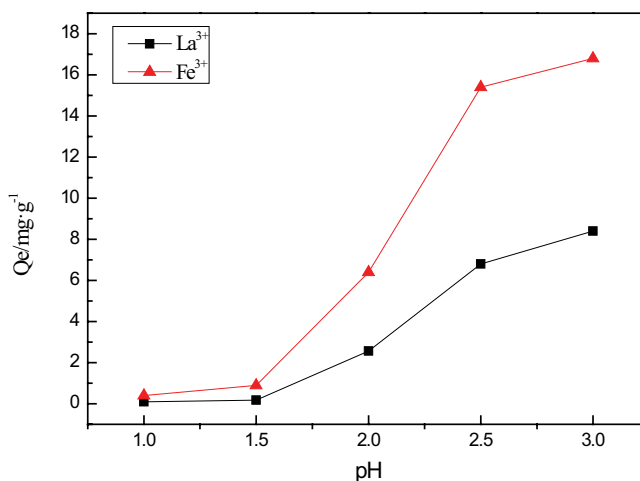


Fig. 6. Effect of pH on adsorption capacity ($T = 25^\circ\text{C}$).

3.6. Adsorption selectivity

The competitive adsorption of Fe(III) in La(III)/Fe(III) mixtures on ACH600 is investigated by the batch method. The relevant results are shown in Table 5. It can be seen that the selectivity coefficient of Fe(III) on ACH600 is 8.3 relative to La(III), indicating that ACH600 has specific recognition selectivity towards Fe(III). This phenomenon is generated from the particularity of the outer electron structure of rare-earth ions and the weaker coordination interaction between La(III) and N atoms compared with that of Fe(III) and N atoms.

3.7. Influence of adsorbent dosage on removal rate of Fe(III)

As seen from Fig. 7, for both single Fe(III) solution and mixed solution of La(III) and Fe(III), the removal rate of Fe(III) increases rapidly with increasing dosage of ACH600 from (38.6%) to (99.9%), beyond which only a slight change can be observed. The removal rate is up to 99% when the dosage of ACH600 is 7.5 g L^{-1} . The sharp increase of removal rate of Fe(III) is ascribed to the increased amount of functional groups on the ACH600 surface. The results show that

Table 5
Distribution coefficient and selectivity coefficient data

Ion	K_d (L/g)	k
Fe(III)	0.83	8.30
La(III)	0.10	

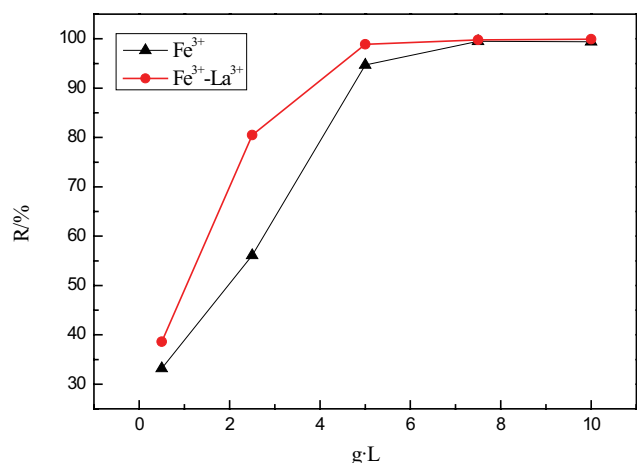


Fig. 7. Removal rate of ACH600 towards Fe(III).

ACH600 could remove Fe(III) efficiently in Fe(III)/La(III) mixed solution.

3.8. Column adsorption characteristics of ACH600 towards Fe(III)

To further demonstrate the selectivity and practical application of ACH600, the solution of Fe(III) and La(III) with an initial concentration of 10 and 100 mg L⁻¹ flowed through ACH600. The adsorption dynamics curve is shown in Fig. 8.

It can be seen from Fig. 8 that the leaking bed volume is 119 BV for Fe and 13 BV for La(III). In addition, the leaking concentration of Fe(III) is less than 5 mg L⁻¹ before 97 BV. This indicates that ACH600 can selectively remove Fe(III) from La(III) solution. This confirms again that ACH600 has high selectivity towards Fe(III).

3.9. Desorption and reusability

In order to further demonstrate the reusability of ACH600, adsorption and desorption experiments of Fe (III) and La (III) on ACH600 were carried out, as shown in Fig. 9.

It can be seen from Fig. 9, the adsorption capacity of ACH600 to Fe(III) almost remains constant during the adsorption/elution process of five cycles, which fully reflects the excellent regeneration and reuse performance of ACH600.

4. Conclusion

In this paper, a novel nitrogen-containing carbon material ACH* was synthesized. The ACH600 has good adsorption ability for Fe(III), and the adsorption capacity can reach up to 15.54 mg g⁻¹. The selectivity coefficient towards Fe(III) is 8.3 and the removal rate is 98.6 %. ACH600 can be used

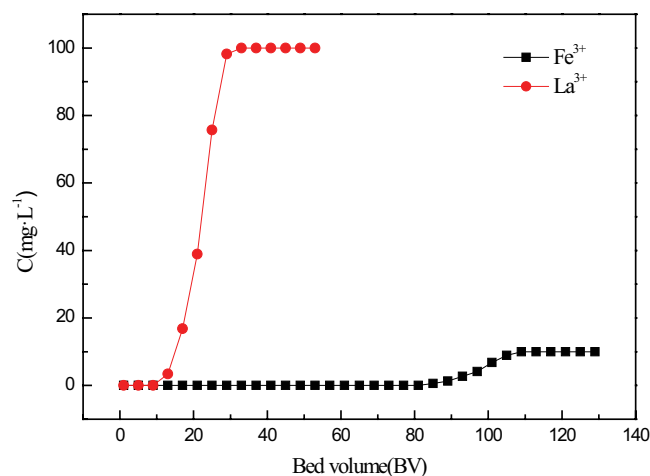


Fig. 8. Dynamic adsorption curve of ACH600 towards a mixture of Fe(III) and La(III).

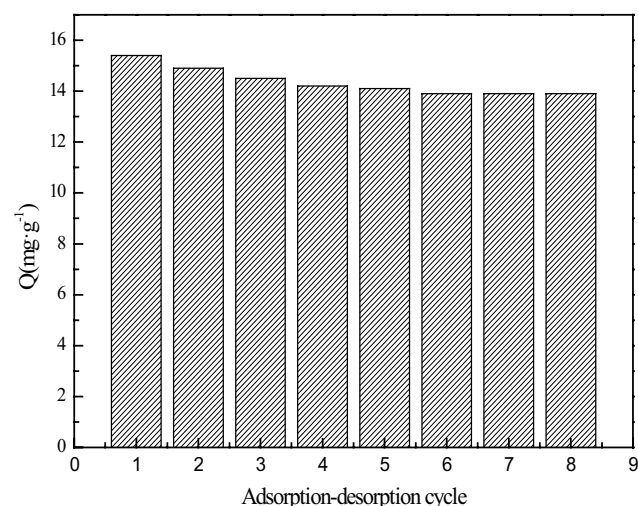


Fig. 9. Adsorption-desorption cycle of ACH600.

as an adsorbent for removing Fe(III) impurities from La(III). In addition, ACH600 could be regenerated using a diluted nitric acid solution as an eluting agent and exhibited excellent reusability. According to the results of this study, the porous activated carbon possesses a promising application in the removal of trace amounts of Fe(III) from La(III).

Acknowledgments

The authors gratefully acknowledge the financial support of this work by the National Natural Science Foundation of China (21676258), Natural Science Foundation of Shanxi Province (201601D102021), Key Research and Development (R&D) Projects of Shanxi Province (201803D31061), and the International Scientific and Technological Cooperation Projects of Shanxi Province (201803D421080), Natural Science Foundation of Shanxi Province (201601D102021, 2015021045).

References

- [1] N.M. Hosny, E. Sayed, E. Morsy, Synthesis spectral, optical and anti-inflammatory activity of complexes derived from 2-aminobenzohydrazide with some rare earths, *J. Rare Earths*, 33 (2015) 758–764.
- [2] V.K. Gupta, A. Rastogi, A. Nayak, Adsorption studies on the removal of hexavalent chromium from aqueous solution using a low-cost fertilizer industry waste material, *Colloid Interface Sci.*, 342 (2010) 135–141.
- [3] Y. Shen, Y.H. Lu, Z. Liu, X. L., X.L. Yu, G.P. Zhang, W.B. Yu, Performance of magneto-optical glass in optical current transducer application, *J. Magn. Magn. Mater.*, 389 (2015) 180–185.
- [4] S.B. Khan, H.M. Marwani, J. Seo, E.M. Bakhsh, K. Akhtar, D. Kim, A.M. Asiri, Poly(propylene carbonate)/exfoliated graphite nanocomposites: selective adsorbent for the extraction and detection of gold(III), *Bull. Mater. Sci.*, 38 (2015) 327–333.
- [5] C.M. Parka, J. Han, K.H. Chu, Y.A.J. Ai-Hamadani, N. Her, J. Heo, Y. Yoon, Influence of solution pH, ionic strength and humic acid on cadmium adsorption onto activated biochar: experiment and modeling, *J. Ind. Eng. Chem.*, 48 (2017) 186–193.
- [6] Z.X. Tan, Y.H. Wang, A. Kasiuliene, C.Q. Huang, P. Ai, Cadmium removal potential by rice straw-derived magnetic biochar, *CLEAN Technol. Environ. Policy.*, 19 (2017) 761–774.
- [7] M.H. El-Naas, S. Al-Zuhair, M.A. Alhaja, Removal of phenol from petroleum refinery wastewater through adsorption on date-pit activated carbon, *Chem. Eng. J.*, 162 (2010) 997–1005.
- [8] M. Essandoh, D. Wolgemuth, C.U. Pittman Jr., D. Mohan, T. Mlsna, Phenoxo herbicide removal from aqueous solutions using fast pyrolysis switchgrass biochar, *Chemosphere*, 174 (2017) 49–57.
- [9] M. Thommes, R. Guillet. Nicolas, K.A. Cychosz, Physical Adsorption Characterization of Mesoporous Zeolites, J. García-Martínez, K. Li, Eds., *Mesoporous Zeolites: Preparation, Characterization and Applications*, Wiley-VCH Verlag GmbH & Co. KGaA, Weinheim, 2015, pp. 349–384.
- [10] X.F. Tan, S.B. Liu, Y.G. Liu, Y.L. Gu, G.M. Zeng, X.J. Hua, X. Wang, S.H. Liu, L.H. Jiang, Biochar as potential sustainable precursors for activated carbon production: multiple applications in environmental protection and energy storage, *Bio-resour. Technol.*, 227 (2017) 359–372.
- [11] C. Zhang, Q. Qiao, J.D.A. Piper, Assessment of heavy metal pollution from a Fe-smelting plant in urban river sediments using environmental magnetic and geochemical methods, *Environ. Pollut.*, 159 (2011) 3057–3070.
- [12] P. Grathwohl, A.D. Zand, Enhanced immobilization of polycyclic aromatic hydrocarbons in contaminated soil using forest wood-derived biochar and activated carbon under saturated conditions, and the importance of biochar particle size, *Pol. J. Environ. Stud.*, 25 (2016) 427–441.
- [13] H.Y. Zhou, Y.L. Wang, X.G. Guo, Y.M. Dong, X. Su, X.Q. Sun, The recovery of rare earth by a novel extraction and precipitation strategy using functional ionic liquids, *J. Mol. Liq.*, 254 (2018) 414–420.
- [14] F.Q. An, B.J. Gao, X.W. Huang, Y.Q. Zhang, Y.B. Li, Y. Xu, Z.G. Zhang, J.F. Gao, Z.P. Chen, Selectively removal of Al(III) from Pr(III) and Nd(III) rare earth solution using surface imprinted polymer, *React. Funct. Polym.*, 73 (2013) 60–65.
- [15] M.K. Jha, A. Kumari, R. Panda, K. Yoo, J.Y. Lee, Review on hydrometallurgical recovery of rare earth metals, *Hydrometallurgy*, 165 (2016) 2–26.
- [16] A. Jain, R. Balasubramanian, M.P. Srinivasan, Production of high surface area mesoporous activated carbons from waste biomass using hydrogen peroxide-mediated hydrothermal treatment for adsorption applications, *Chem. Eng. J.*, 273 (2015) 622–629.
- [17] P. Davris, S. Stopic, E. Balomenos, D. Pánias, I. Paspaliaris, B. Friedrich, Leaching of rare earth elements from eudialyte concentrate by suppressing silica gel formation, *Miner. Eng.*, 108 (2015) 115–122.
- [18] A.M. Puziy, M. Poddubnaya, O.I.A. Martínez-Alonso, F. Suarez-García, J.M.D. Tascon, Surface chemistry of phosphorus-containing carbons of lignocellulosic origin, *Carbon*, 43 (2005) 2857–2868.
- [19] T. Ahmad, M. Danish, M. Rafatullah, A. Ghazali, D. Sulaiman, R. Hashim, M.N.M. Ibrahim, The use of date palm as a potential adsorbent for wastewater treatment: a review, *Environ. Sci. Pollut. Res.*, 19 (2012) 1464–1484.
- [20] P.G. González, Y.B. Pliego-Cuervo, Adsorption of Cd(II), Hg(II) and Zn(II) from aqueous solution using mesoporous activated carbon produced from bambusa vulgaris striata, *Chem. Eng. Res. Des.*, 92 (2014) 2715–2724.
- [21] F. Gao, D.L. Zhao, Y. Li, X.G. Li, Preparation and hydrogen storage of activated rayon-based carbon fibers with high specific surface area, *J. Phys. Chem. Solids*, 71 (2010) 444–447.
- [22] J. Lee, J. Kim, T. Hyeon, Recent progress in the synthesis of porous carbon materials, *Adv. Mater.*, 18 (2011) 2073–2094.
- [23] J.C. Moreno-Piraján, R. Gómez-Cruz, V.S. García-Cuello, L. Giraldo, Binary system Cu(II)/Pb(II) adsorption on activated carbon obtained by pyrolysis of cow bone study, *J. Anal. Appl. Pyrolysis*, 89 (2010) 122–128.
- [24] C.L. Qi, M.W. Meng, Q.Y. Liu, C.Y. Kang, S.Y. Huang, Z.M. Zhou, C.Q. Chen, Adsorption thermodynamics and kinetics of auramine O on sugarcane leaves activated carbon, *J. Funct. Biomater.*, 46 (2015) 2048–2052.
- [25] G.L. Ou, J.F. Gao, T.P. Hu, F.Q. An, Y. Wang, Y.J. Wang, D. Zhong, Synthesis of an activated carbon based urea formaldehyde resin and its adsorption and recognition performance towards Fe(III), *RSC Adv.*, 5 (2015) 71878–71882.
- [26] F.Q. An, R.Y. Wu, M. Li, Z.G. Yuan, T.P. Hu, J.F. Gao, Selective removal of Al(III) from rare earth solutions using peas-based activated carbon, *J. Korean Chem. Soc.*, 61 (2017) 231–237.
- [27] A. Üçer, A. Uyanik, Ş.F. Aygün, Adsorption of Cu(II), Cd(II), Zn(II), Mn(II) and Fe(III) ions by tannic acid immobilised activated carbon, *Sep. Purif. Technol.*, 47 (2006) 113–118.
- [28] M. Sumrit, M. Phansiri, P. Wanwimon, K. Sataporn, Characterization and properties of activated carbon prepared from tamarind seeds by KOH activation for Fe(III) adsorption from aqueous solution, *Sci. World J.*, 2015 (2015) 9p, <https://doi.org/10.1155/2015/415961>.
- [29] X.H. Zhu, J. Li, Y. Jin, Y.H. Guo, Preparation of porous hybrid adsorbents based on fluor(calcium silicate)/activated carbon and its application in the removal of iron(III) from ammonium phosphate solutions, *Arab. J. Chem.*, 13 (2020) 1551–1562.
- [30] P. St. Vassileva, Albenak, K. Detcheva, Adsorption of some transition metal ions [Cu(II), Fe(III), Cr(III) and Au(III)] onto lignite-based activated carbons modified by oxidation, *Adsorpt. Sci. Technol.*, 28 (2010) 229–242.
- [31] R. Chand, T. Watari, K. Inoue, Hidetaka, H.N. Luitel, D. Parajuli, Selective adsorption of precious metal from hydrochloric acid solutions using porous carbon prepared from barley straw and rice husk, *Miner. Eng.*, 22 (2009) 1277–1282.
- [32] W.X. Zhou, T.P. Hu, J.F. Gao, X. Chen, W.G. Ping, C.C. Wei, F.Q. An, Synthesis of high-performance nitrogen-containing porous carbon and adsorption properties towards metal ions, *Desal. Wat. Treat.*, 57 (2016) 4494–4501.
- [33] F.Q. An, R.Y. Wu, M. Li, Z.H. Yuan, T.P. Hu, J.F. Gao, Recognition performance and mechanism of the activated carbon based UF resin towards traces of Fe(III) in rare earth solutions, *Environ. Chem. Eng.*, 5 (2017) 1638–1644.